AMB System for Rotordynamic Experiments: Calibration Results and Control

P. Förch*, C. Gähler**, R. Nordmann*

*Mechatronische Systeme im Maschinenbau, TH Darmstadt,
Petersenstr. 30, 64287 Darmstadt, Germany
e-mail: foerch@mesym.th-darmstadt.de

**International Center for Magnetic Bearings, ETH Technopark,
Technoparkstr. 1, 8005 Zürich, Switzerland
e-mail: gaehler@ifr.mavt.ethz.ch

Abstract: An AMB system designed especially for rotordynamic experiments has been developed. It allows selective sinusoidal excitation of forward and backward modes of the free rotating rotor, as well as the simulation of unbalance forces. A main requirement is precise force measurement. This has been achieved using flux measurement by means of Hall sensors. Much attention has been paid to assessing the force measurement accuracy. Results are included. Furthermore, a new controller design method for AMB systems with highly flexible and gyroscopic rotors is presented.

1 Introduction

Modal testing methods for non-rotating structures are well developed. For a turbomachinery user, however, it is very important to get information also about the dynamic behaviour of the machinery in rotating state [1]. In practice it is usual to measure the output frequency spectrum of rotating structures. Vibrational amplitudes can be measured in this way; but only limited information about vibrational properties can be obtained, because the exciting forces are not known.

Vibrational properties can be assessed if frequency response functions are measured. They can be described in terms of modal parameters (natural frequencies ω_r, modal dampings c_r, and mode shapes Φ_r), which together form a modal description of the rotating structure. These parameters can then be compared with the modal parameters obtained from a Finite Element model of the structure. They can also be used to update the Finite Element model.

It is therefore a goal of the BRITE/EURAM project MARS[1] [1] (Modal Analysis of Rotating Structures) of the European Community to develop methods for modal analysis for rotating structures. A test rig for rotordynamic experiments has been developed for this purpose (figure 1). Magnetic bearings are an important part of this test stand. They offer the possibility to excite the rotor in arbitrary direction while keeping the rotor floating. The key figures of the AMB as an exciter are listed below.

Key figures of the magnetic bearing exciter:

- Maximum force: F_{max} = 800 N
- Dynamic force : sinusoidal force with amplitude F_{max} = 200 Hz can be achieved up to 800 N
- Inner stator diameter = 116 mm
- Nominal air gap: s_0 = 0.8 mm

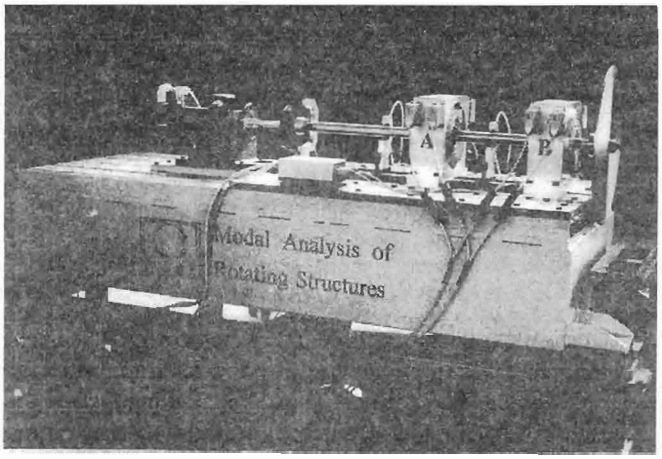

Figure 1: MARS test rig

Outline of the Paper

Precise force measurement is crucial for precise measurement of the rotor's vibrational behaviour. Therefore the presented AMB system was optimised in this respect. The principle is shortly summarised in section 2. The methods used to calibrate and to validate the force computation are presented in section 3. Section 3.2 contains the resulting characteristics. Section 4 presents the main output of the test stand: High quality measurements of the frequency response function (FRF) of the rotating rotor. The test rotors have deliberately been designed highly flexible (9 flexible modes below the Nyquist frequency at 2.3 kHz) and

[1] BRITE/EURAM project nr. 5464.-92.
„Development of Validated Structural Dynamic Modelling and Testing Techniques for Vibration Predictions in Rotating Machinery"
The project partners are:
- Imperial College London, UK (Prof. D. J. Ewins)
- ETH Zurich, Switzerland (Prof. G. Schweitzer)
- TH Darmstadt, Germany (Prof. R. Nordmann)

highly gyroscopic (the first two flexible eigenfrequencies vary by ±20 % between standstill and nominal rotational speed). Position control therefore required new considerations and approaches. These results are presented in section 5.

2 Excitation and Force Computation

In conventional bearing applications, the controlled variable is the displacement. When using the AMB as an exciter the controlled variable is the force. The displacement can be considered mainly as a disturbance input. The main requirement to the AMB is that the force can accurately set and, even more important, accurately measured, i.e., computed from appropriate measurements.
In particular, the force measurement should not be corrupted by

- iron saturation, eddy current, hysteresis, sensor and actuator dynamics
- manufacturing inaccuracies, for operation with different rotors
- not centered rotor position and misalignment if the rotor is mounted in roller bearings

The force measurement must also be accurate when

- the rotor is displaced by the excitation
- there is a bias force (for supporting the rotor with AMB's) and the bias force is different for several rotor configurations
- the magnetic bearing amplifier is not calibrated accurately

2.1 Principles of AMB Force Measurement

There are three main principles to measure the magnetic bearing force:

1) Compute the force from the coil current and displacement with

$$F(x,i) = k_i \cdot i + k_s \cdot x \qquad (1)$$

Equation (1) becomes inaccurate when the displacement amplitude is large comparing to the air gap. However considerable displacement must be assumed when the rotor is deliberately excited. Furthermore, saturation, hysteresis, and eddy current effects cannot be taken into account.

2) Measure the force between AMB housing and foundation using piezoelectric quartz elements [3] and assume the bearing force acting on the rotor to be equal to the measured force. The difficulty is to calibrate the quartz elements accurately, including cross coupling effects between all force directions and the respective output signals of the quartz probes. Also, the quartz probes have a certain compliance which allows the bearing stator to vibrate. The resulting inertia forces distort the measured result, especially for higher frequencies. Accelerometers mounted on the bearing stators can be used to compensate this error.
3) Compute the force from flux measurement, using

$$F \sim \Phi^2 \qquad (2)$$

for each pole of the bearing. Equation (2) is correct also in the presence of saturation, eddy current and hysteresis effects. Because this principle can be expected to yield the best accuracy, it was selected for the MARS test rig.

2.2 Force Computation from Magnetic Flux Density

In order to accommodate the Hall sensors in the air gap, the air gap s_0 must be widened by $\varepsilon_0 = 1$ mm. With given ampere turns, this reduce the maximal force. Furthermore, the hardware complexity is increased (additional analog inputs). As a compromise, it was decided to place Hall effect sensors only at the north poles. To reduce stray flux caused by this asymmetry, the pole pairs must be separated by a large air gap s_y. This resulting geometry is shown in figure 2. The flux in the south poles is not equal to the flux of the north poles, because there is still a stray flux between the pole pairs. However, it can be approximated in real time from the measured fluxes and the rotor position. This approximation is based on a magnetic resistor network model (figure 3) [2].

3 Magnetic Bearing Force Calibration

3.1 Set-up and Procedure

An important step of the commissioning process was the precise calibration of gains and offsets of Hall sensors and position sensors. Furthermore, the quality of the force measurement was characterised and validated. Calibration was done statically; validation was done both statically and

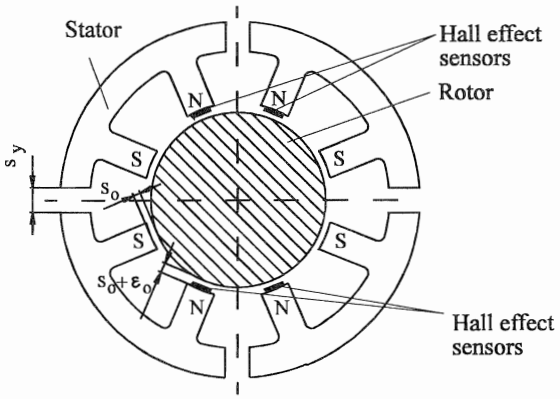

Figure 2: Pole pair geometry

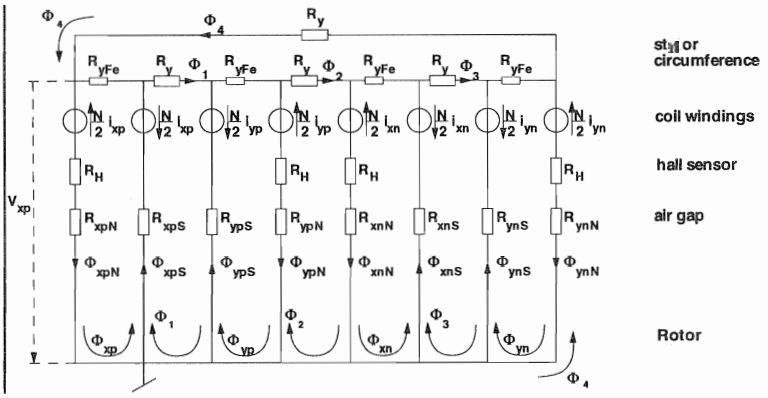

Figure 3: Resistor network diagram

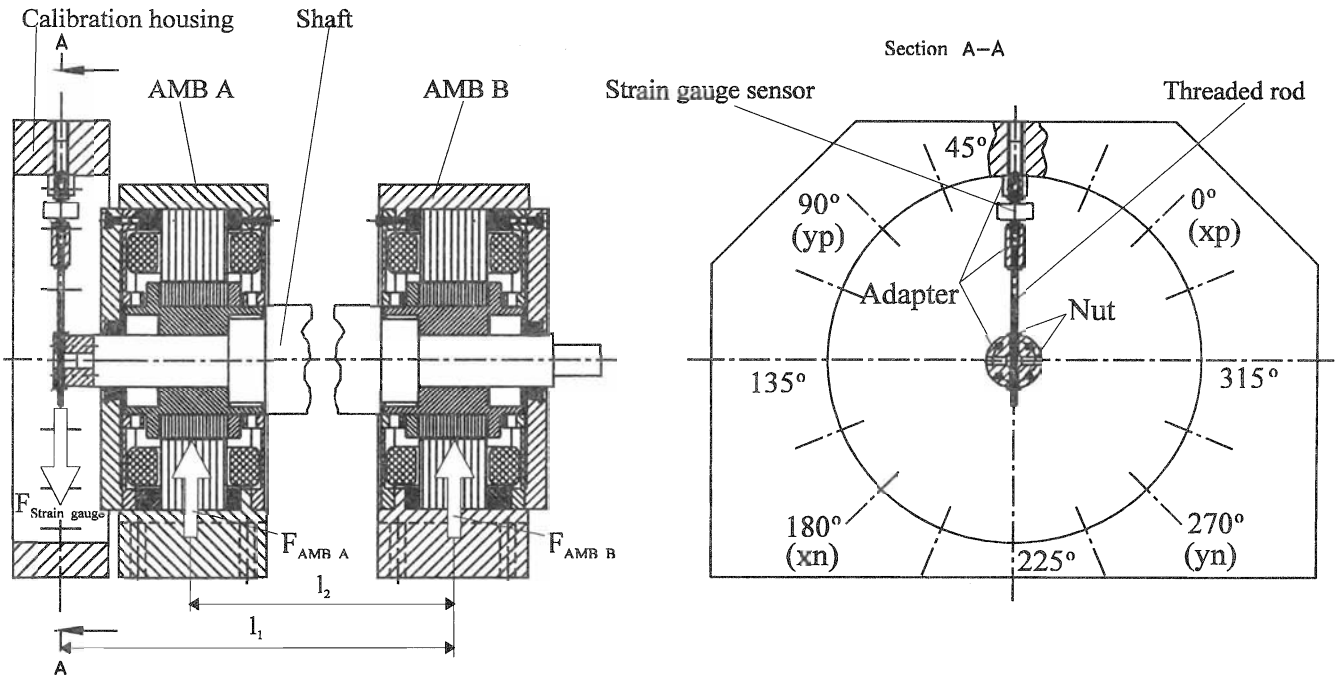

Figure 4: Static Calibration Set-up

dynamically. We will restrict the description to the validation process.

Static validation allowed to asses linearity and hysteresis of the force measurement method. Experiments included comparison of the force measurement

a) with known test forces, when the rotor was at nominal position
b) with known test forces, when the rotor was at a constant position displaced from nominal position
c) with unknown constant test forces, when the rotor was slowly moved on orbits around the air gap.

Dynamic calibration allowed to check the correctness of the force measurement with varying frequency. It was done by measuring the multivariable transfer function from force to acceleration with varying frequency.

Static Calibration: For experiments a) and b), known static forces were applied to the rotor via a strain gauge load cell in all radial directions. Figure 4 shows the experimental set-up. The strain gauge sensor was fixed by means of a threaded rod between the rotor and the bearing housing. It could be positioned in different directions. Two nuts allowed to vary the test force within the limits of the AMB capacity, i.e., between -800 N ... 800 N. In this way, complete hysteresis cycles were measured.

For experiment c), the load force was applied to the rotor via soft springs while it was moved slowly on a circular orbit within the air gap.

The force error was always measured in parallel with and perpendicular to it.

Dynamic Calibration: A "rigid" dummy rotor that did not exhibit resonance frequencies within the measurement range of 0...200 Hz was used for the entire calibration and validation process. The accelerations were computed in frequency domain from the measured displacements with

$$\boldsymbol{a}(j\omega) = -\omega^2 \cdot \boldsymbol{x}(\omega) \tag{3}$$

The transfer function from force to acceleration is defined by

$$\boldsymbol{a}(j\omega) = \boldsymbol{H}(j\omega) \cdot \boldsymbol{F}(j\omega) \tag{4}$$

where

$$\boldsymbol{a} = \left[a_{xA} \quad a_{xB} \quad a_{yA} \quad a_{yB}\right]^T \tag{5}$$

$$\boldsymbol{F} = \left[F_{xA} \quad F_{xB} \quad F_{yA} \quad F_{yB}\right]^T \tag{6}$$

for a rigid rotor, $\boldsymbol{H}(j\omega)$ is equal to its inverted mass matrix and thus constant with frequency.

3.2 Calibration and Validation Results

The accuracy of the force measurements can be summarised as follows:

Static force accuracy:

- Linearity error including hysteresis (cf. figure 5)
  1.5 % up to ±500 N
  3 % up to ±800 N
- Hysteresis
  Worst case direction (horizontal force, cf. figure 6):
  < ±2.5 N (0.5%) up to ±500 N force amplitude
  < ±4 N (0.5%) up to ±800 N "
  Best case direction (vertical direction, cf. figure 5):
  < ±1.5 N (0.2%) up to ±800 N "
- Error caused by displacement at a load of 800 N (cf. figure 8)
  5 N (0.6%) at 0.1 mm displacement
  10 N (1.2%) at 0.15 mm displacement
  20 N (2.5%) at 0.3 mm displacement

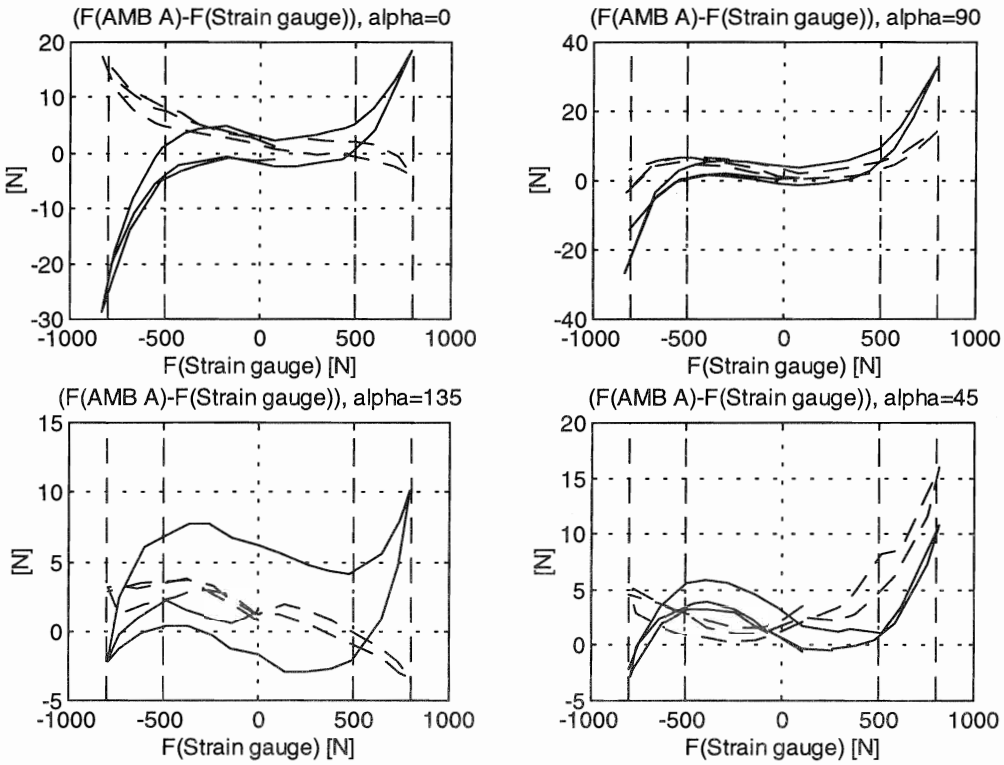

Figure 5: Force error at AMB A with static calibration method a) in four directions. the solid and dotted lines denote the force errors in parallel with and perpendicular to the load, respectively. The direction angle refers to figure 4.

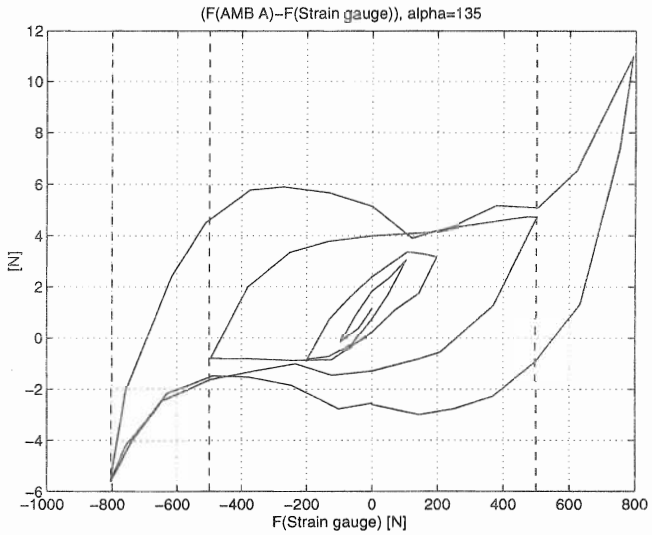

Figure 6: Hysteresis for force amplitudes of 100, 200, 500, and 800 N, with load in horizontal direction (worst case)

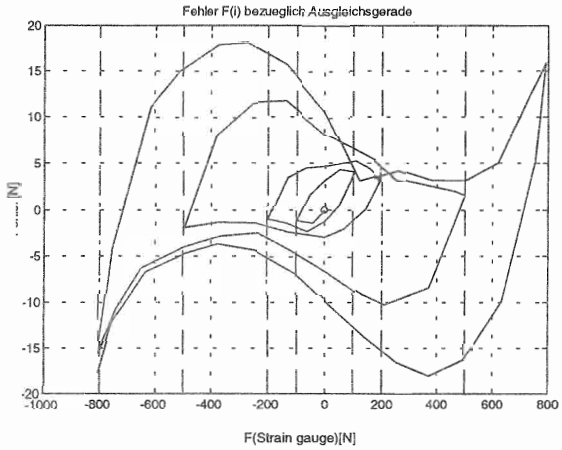

Figure 7: Hysteresis F(i,x) for comparison to figure 6

Dynamic force measurement accuracy[2]:

Linearity (excitation amplitudes 10...450 N, 120 Hz, cf. figure 9)

- Amplitude error (variation): ±1%
- Phase error (variation): ±0.5°

Frequency dependence, 30...190 Hz

- Amplitude error: ±5.5%
- Phase errror: < 2°

2 The error in the transfer function below 30 Hz, is due to low force amplitude combined with large displacement. The reduction of the measured transfer function above 190 Hz is mainly due to a resonance of the bearing stator carrying the displacement probes. We can assume that in reality, the force measurement accuracy would be much better above 190 Hz than what the plot suggests.

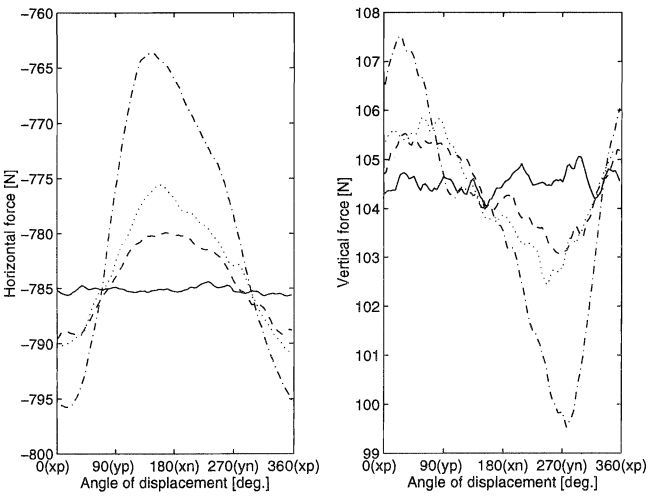

Figure 8: Force error with constant load (ca. 800 N) in horizontal direction. The rotor was moved slowly on orbits with radius of 0, 0.1, 0.15, 0.3 mm

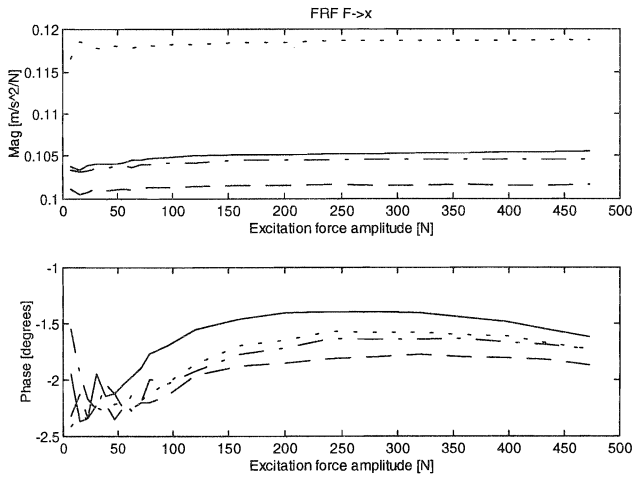

Figure 9: Linearity for excitation amplitudes of 10...450 N at 120 Hz excitation frequency

3.3 Comparison to F(i,x)

Since the presented force measurement method is more expensive than force computation from current and displacement according to equation (1), the performance of the two methods has been compared. Some characteristics of the method (1) are listed below (figure 7).

Hystseresis: max. ±11 N (1.5%) (cf. with Hall sensors: max. ±4N)

Static linearity error: Clearly worse than with Hall sensor measurement.

Linearity[3] (excitation amplitudes 10...450 N, 120 Hz)

- Amplitude error (variation): ±7%
- Phase error (variation): ±2°

As can be seen from comparison with the figures from section 3.2, the presented force measurement using Hall sensors performs clearly better. A hysteresis of 2% shows also a measurement presented in [6] using method 1.

3.5 Sources of Force Measurement error

The force computation based on (2) should yield correct force values. However, the approximation of the non-measured flux in the south poles is not perfectly accurate mainly due to the following reasons:

- The force computation method implemented in the MARS AMB exciter is based on an approximation based on a magnetic resistor network built from lumped parameters. The lumped parameter model provides valuable insight into the system behaviour but cannot model the stray fluxes precisely.
- The flux amplitudes in north and south poles are not equal. Therefore the hysteresis amplitudes are different also. This cannot be taken into account with the presented system.

4 FRF Measurement Results

Frequency response functions allows to assess the vibrational properties. Figure 10 gives an impression about the quality of the FRF's. The rotor is rotating with a speed of 2000 rpm. A stepped sine excitation in x direction at bearing A around the second resonance demonstrate the gyroscopic split of the system. The two resonances shows the second backward and forward modes.

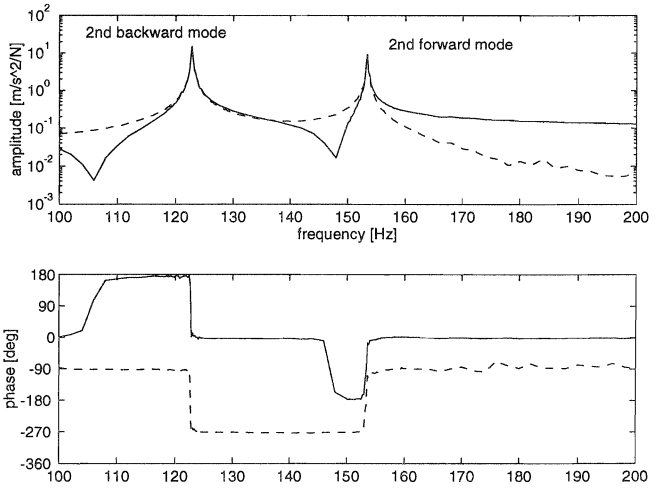

Figure 10: FRF of the rotor at 2000 rpm. Solid line : Response in xA direction; Dashed line: Response in yA direction

5 Position Control for Highly Flexible and Gyroscopic Rotors

5.1 The plant's dynamics

The design of a controller for the MARS test stand proved to be quite tricky, although the nominal speed is as low as 3000 rpm (50 Hz). The reasons are:

- The rotor is highly flexible: There are 9 flexible modes up to the Nyquist frequency at 2.3 kHz.

[3] The measured transfer function i → a (current to acceleration) has been used for this comparison.

- The rotor is highly gyroscopic: The large disk on the slender shaft causes the first two eigenfrequencies to vary by ±20% between 0 and 3000 rpm.
- The first backward mode drops lower than 50 Hz at nominal speed and must therefore be well damped.
- The bias current required to achieve the maximal force of 800 N causes the AMB to have a high k_S. Therefore, a high static controller gain is required.

The rotor was deliberately designed to have all these nasty properties, since the investigation of gyroscopic effects on flexible eigenmodes is a main goal of the MARS project. It is therefore not a viable option to "improve" the mechanical side.

We will restrict ourselves to the discussion of the configuration with "rigid" disk in this paper. The first four eigenfrequencies (backward/forward modes) [Hz] of the free rotor are:

	1st mode	2nd mode	3rd mode	4th mode
standstill	58.2	136	332	508
3000 rpm	45.2/72.4	120/168	324/343	502/516

For comparison, the largest real rigid-body pole pair is at ±42.6 Hz in standstill. Its absolute value is almost as large as the first flexible eigenfrequency

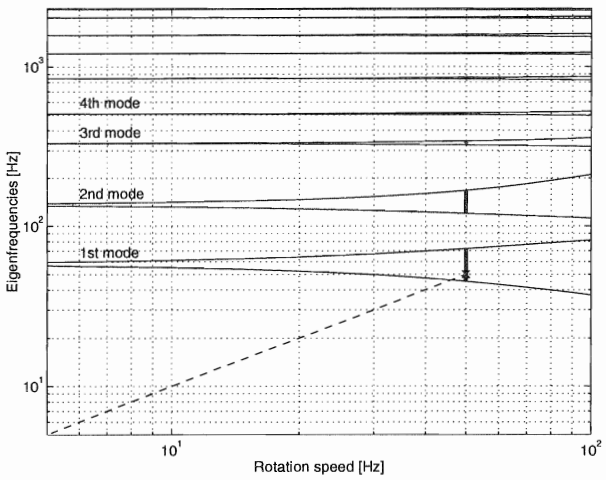

Figure 11: Campbell diagram of the free rotor

5.2 Criteria and guidelines for controller design

We restricted ourselves to decentralised control. This accounts for the limited computational power, and makes the design process described subsequently somewhat more transparent. The two controllers associated with x and y directions at the same bearing are equal (rotational symmetry). Furthermore, the controller should not depend on the revolution speed of the rotor.

The sampling time was 220 µs, corresponding to a Nyquist frequency of 2.3 kHz.

The "performance criterion"

To assess the controller performance we use the closed-loop poles: All closed-loop poles must be stable in the whole range of revolution speeds. A certain robustness and performance can be assumed if they are not too close to the stability boundary. This is not a sophisticated but a practical criterion to assess the controller's performance.

Requirements to the open-loop controller transfer function

We can establish a list of necessary - but not sufficient - requirements that the open-loop transfer function of the controller must satisfy:

a) **PD characteristics at low frequencies:** At low frequencies, the controller gain must be sufficiently large to overcompensate the negative bearing stiffness. The controller phase must be positive ($0°<\varphi<180°$) to damp the rigid body modes. In short, in the low frequency range, the controller must have a PD characteristic to stabilise the rigid body modes.

b) **Low gain at high frequencies:** It has been stated that an ideal PD controller could stabilise a current-controlled AMB system even in the presence of flexible modes and gyroscopic effects. This is true but only of theoretical value. In reality, the amplifier gain must be limited at high frequencies because of many strong reasons. Some of them are:

- α) Realisation: Ideal PD controllers cannot be realised, neither in analog nor in digital way.
- β) Robustness: The plant model uncertainty increases with frequency. A controller with high gain at very high frequencies would therefore not stabilise the AMB plant robustly. Robust control is only possible if the controller gain is limited at high frequencies. For high frequencies, the controller gain must therefore be "reasonably" small.
- γ) Avoidance of actuator saturation: The voltage limitation of the power amplifiers limits the achievable current slope. High frequency noise will easily drive the amplifiers into voltage saturation if the controller's high frequency gain is too high.
- δ) Aliasing with rotor resonances around the Nyquist frequency: With digital control, if there are eigenfrequencies both closely below and above the Nyquist frequency, a controller with high gain at the Nyquist frequency will inevitably destabilise either of them. Anti-aliasing filter cannot help because they have a limited roll-off.

c) **Damping of flexible eigenmodes:** We will first consider the case of collocation[4]. Active control can then damp flexible eigenmodes if the controller phase is positive at the related eigenfrequencies. Conversely, the controller can destabilise an eigenmode if the phase is wrong.

4 Collocation means in this context that the rotor's displacement is measured exactly at the actuator location, i.e., at the middle of the bearing.

5.3 How to combine damping with low HF gain? Active damping with negative phase

With PD control, damping is provided in the frequency band where the controller phase $\varphi > 0°$. Unfortunately, the controller gain inevitably increases with frequency as long as the phase is positive. Conversely, the controller phase will necessarily become negative where the controller gain decreases with frequency[5]. The requirement of low HF gain inevitably leads to a negative phase above a certain frequency. However, with the MARS rotors, there are many closely spaced eigenfrequencies up to the Nyquist frequency. Therefore the question arises as to how these can be actively damped.

The answer lies in a wrap-around of the controller phase: If the phase drops below -180°, the damping becomes positive again. More generally speaking: The controller damps an eigenmode if its phase lies in an interval [0°...180°], [-360°...-180°], [-720°...-540°], ... at the corresponding eigenfrequency, and tends to destabilise it otherwise. Therefore, if we succeed in driving the controller phase from >0° to <-180° between two resonance frequencies of the rotor, we can expect that the controller will stabilise the rotor: All eigenmodes can then be damped.

Obviously, a low pass filter of at least order 3 is needed to realise a phase transition of more than 180 degrees. In fact, Matsushita proposed a PD controller with 3rd order low pass filter [7]. He applied this controller to a system with a flexible rotor supported by one AMB and one ball bearing in non-rotating state. This idea was now extended to the presented multivariable control problem including robustness with respect to speed variation.

5.4 Robustness to speed variation

Variation of the rotational speed causes the rotor's resonance frequencies to vary over a certain range. With collocation, the above-mentioned phase transition must take place between two resonance frequencies for all rotational speeds, *i.e.*, between two resonance frequency ranges. The prohibited resonance frequency ranges are visualised by thick vertical lines at the maximal speed of 3000 rpm (50 Hz) in the Campbell diagram, and lie between dash-dotted vertical lines in the Campbell diagram (figure 11).

5.5 Higher order low-pass filters

The best place for the phase transition can be expected to be where the gap between two resonance frequency ranges is largest in logarithmic scale. This is the gap between the 2nd and the 3rd flexible eigenmode of the rotor.

Unfortunately, the phase transition achievable with a 3rd order low-pass filter proves to be too smooth to fit into this gap. A low-pass filter of higher (e.g., 4th) order can solve this problem. In fact, such a controller can well stabilise the rotor's poles. However, the AMB plant always destabilises some of the low pass filter poles with our plant, no matter where they are placed.[6]

5.6 Making use of non-collocation

Apparently, the problem is that the gap between the resonance frequency ranges is too narrow. Use of non-collocation can help to circumvent this problem.

Non-collocation means that the position sensors are placed beside (and not at) the bearing. If a particular eigenform has a node between sensor and middle of the bearing, the phase conditions established in section 5.2 are reverted. The controller will then help stabilising this eigenmode if its phase is in one of the intervals [-180°...0°], [-540°...-360°], ..., and tend to destabilise it otherwise. This mode may then lie within the phase transition range, which allows smoother phase transition.

It is a main result of the presented work that non-collocation can help to find a stabilising controller.

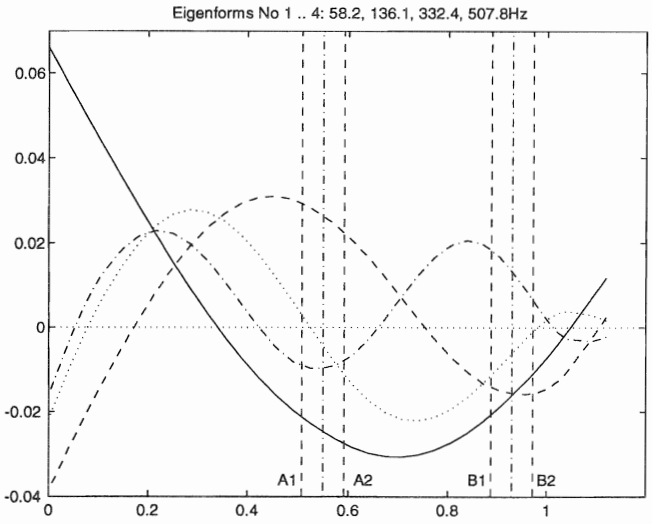

Figure 12: Eigenforms of the free rotor. The solid, dashed, dotted, and dash-dotted lines denote the first four eigenforms. The dash-dotted vertical lines denote the bearing midpoints, the dashed lines denote the sensor locations.

5.7 Refinements

The phase conditions of section 5.2 and 5.3 holds for analog control without dead time. Sampling of the plant, anti-aliasing filters and plant dead time must be included. These three effects all cause additional phase lag for the plant, which we subsequently denote by $\varphi_a(\omega)$. Consequently, the controller phase must be increased by φ_a to stabilise the system. To determine whether the controller has a damping or a destabilising influence on a particular mode, its phase must therefore no longer be refered to 0°, -180°, -360° ...

---

5 More precisely, even worse: The phase will be negative where the controller gain has its maximum value.

6 This statement must be understood in the sense of the root locus map with increasing controller gain: While the open-loop poles of the plant become stable with increasing controller gain, the open-loop poles of the controller become unstable.

but to the reference phases $0°+\varphi_a$, $-180°+\varphi_a$, $-360°+\varphi_a$[7] (cf. figure 13).

5.8 The realised controller

In the MARS test stand, there are two sensor planes per bearing, both to the left and to the right hand side of each bearing. It can be decided by software for each bearing to use sensor plane 1 only, sensor plane 2 only, or the average (collocation).

The 3rd eigenmode has a node between sensor plane A1 and the middle of bearing A. Therefore, sensor plane 1 is used for bearing A. The phase transition of controller A can then be quite smooth between modes 2 and 4. This allows effective damping of mode 2, due to a comfortable margin to the reference phase, and also effective damping of mode 3. Controller B has a destabilising impact on the second forward mode at higher rotational speeds, but this is overcompensated by controller A. It yields significant damping to mode 4, which cannot be damped well with controller A.

The PD controller with 3rd order low pass filter is only the main ingredient for the controller. A complex-conjugate pole/zero pair (a kind of complex lead/lag or lag/lead, respectively) had to be added to both controllers to further adjust the controller phase in the vicinity of the 2nd and 3rd rotor resonance frequencies. A zero on the negative real axis in the z domain also proved to be helpful. So, the design process ended up with 6th order controllers for both bearings.

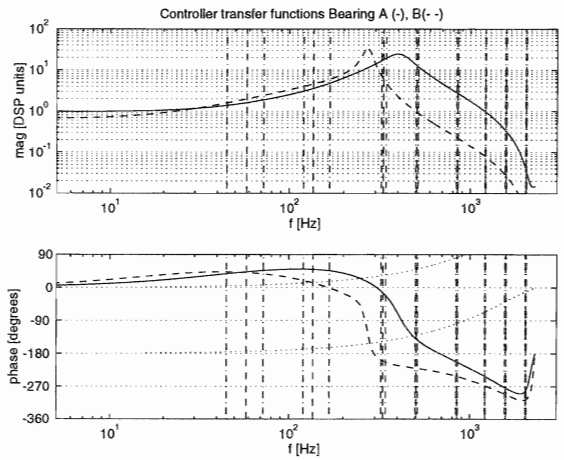

Figure 13: Bode diagram of the realised controllers. Solid: Controller for bearing A; dashed: Controller for bearing B. The dashed vertical lines denote the rotor resonance frequencies at 0 rpm, the dash-dotted vertical lines denote the backward and forward resonances at 3000 rpm. The resonance frequency ranges lie between the dash-dotted vertical lines. The dotted lines starting at 0 and -180 denote the reference phases delimiting the controller phase ranges where eigenmodes will be damped or destabilised, respectively.

6 Conclusions and Outlook

An AMB system for generating excitation forces has been developed. The accuracy of the used force measurement method has been validated with several calibration methods. The results of the calibration shows the advantages against common used force measurement methods. For the highly flexible and gyroscopic structure a special controller design has been developed. Magnetic bearings offer the possibility for continuos determination of vibrational properties in operating condition. In the future, this can be used for on-line diagnosis in rotating machinery.

Acknowledgements

The presentation is a result from research work which was supported by the European Community and the Swiss 'Bundesamt für Bildung und Wissenschaft' in the scope of the BRITE/EURAM program. Special thanks to all project partners for many helpful discussions and contributions.

References

[1] Nordmann, R.; Matros, M.; Neumer, T.: Parameter Identification in Rotating Machinery by Means of Active Magnetic Bearings. IFTOMM, 4th Conference on Rotor Dynamics, Chicago, Illinois, 1994

[2] Gähler, C.; Förch, P.: A Precise Magnetic Exciter for Rotordynamic Experiments. Fourth Int. Symposium on Magnetic Bearings, August 1994, Zurich, Switzerland.

[3] Lee, C.-W.; Kim J.-S.: Modal Testing and suboptimal Vibration Control of Flexible Rotor Bearing Systems by Using a Magnetic Bearing. Journal of Dynamic Systems, Measurements and Control, Vol. 114 p. 244-252, June, 1992

[4] Schweitzer, G.; Bleuler, H.; Traxler, A.: Active Magnetic Bearings. Verlag der Fachvereine, Zurich, Switzerland, 1994

[5] Traxler, A.: Eigenschaften und Auslegung von berührungsfreien elektromagnetischen Lagern. Diss. ETH Zurich Nr. 7851, 1985

[6] Pottie, K.; Wallays, G.; Verhoeven, J.; Sperry, R.; Gielen, L. De Vies, D., Neumer, T.; Matros, M.; Jayawant R.: Active Bearings used in BW/IP Centrifugal Pumps. Fourth Int. Symposium on Magnetic Bearings, August 1994, Zurich, Switzerland.

[7] Matsushita, O.; Takahashi, N.; Takagi, M.: Third order LPF Type Compensator for Flexible Rotor Suspension. Third Int. Symposium on Magnetic Bearings, Alexandria VA, USA, 1992

---

7 φ_a (phase of the sampled anti-aliasing filter) can be computed as

$\varphi_a = \omega \cdot T_d$.

where T_d is the dead time of the system.